Institute of Paper Science and Technology
Atlanta, Georgia

IPST Technical Paper Series Number 640

Dynamic Simulation of Particles Suspended in Fluid

C.K. Aidun, Y. Lu, and E.-J. Ding

February 1997

Submitted to
ASME Fluids Engineering Division Summer Meeting
Vancouver, British Columbia, Canada
June 22–26, 1997

INSTITUTE OF PAPER SCIENCE AND TECHNOLOGY
PURPOSE AND MISSIONS

The Institute of Paper Science and Technology is a unique organization whose charitable, educational, and scientific purpose evolves from the singular relationship between the Institute and the pulp and paper industry which has existed since 1929. The purpose of the Institute is fulfilled through three missions, which are:

- to provide high quality students with a multidisciplinary graduate educational experience which is of the highest standard of excellence recognized by the national academic community and which enables them to perform to their maximum potential in a society with a technological base; and
- to sustain an international position of leadership in dynamic scientific research which is participated in by both students and faculty and which is focused on areas of significance to the pulp and paper industry; and
- to contribute to the economic and technical well-being of the nation through innovative educational, informational, and technical services.

ACCREDITATION

The Institute of Paper Science and Technology is accredited by the Commission on Colleges of the Southern Association of Colleges and Schools to award the Master of Science and Doctor of Philosophy degrees.

NOTICE AND DISCLAIMER

The Institute of Paper Science and Technology (IPST) has provided a high standard of professional service and has put forth its best efforts within the time and funds available for this project. The information and conclusions are advisory and are intended only for internal use by any company who may receive this report. Each company must decide for itself the best approach to solving any problems it may have and how, or whether, this reported information should be considered in its approach.

IPST does not recommend particular products, procedures, materials, or service. These are included only in the interest of completeness within a laboratory context and budgetary constraint. Actual products, procedures, materials, and services used may differ and are peculiar to the operations of each company.

In no event shall IPST or its employees and agents have any obligation or liability for damages including, but not limited to, consequential damages arising out of or in connection with any company's use of or inability to use the reported information. IPST provides no warranty or guaranty of results.

The 1997 ASME Fluids Engineering Division Summer Meeting
FEDSM'97
June 22-26, 1997

FEDSM97-3181

DYNAMIC SIMULATION OF PARTICLES SUSPENDED IN FLUID

Cyrus K. Aidun*, Yannan Lu, and E-Jiang Ding
Institute of Paper Science and Technology, 500 10th Street, N.W., Atlanta, GA 30318

ABSTRACT

We have developed an efficient computational method for hydrodynamic analysis of solid particle(s) suspended in fluid. After a brief outline of the numerical technique, we demonstrate the accuracy and robustness of our method by comparing the results with (1) the asymptotic solutions at small particle Reynolds number, $Re_p \ll 1$, for particle sedimentation and particles suspended in shear flows, (2) 2-D Finite Element simulations of single and multi-particle sedimentation at finite Re_p, and (3) experimental results. We present new results from 3-D computational analysis of solid particle(s) sedimentation. The emphasis of this paper is on demonstration of the accuracy, robustness, and computational efficiency of our approach. Some new 2-D and 3-D results for sedimenting ellipses and prolate spheroids will also be presented. The results indicate that the sedimentation dynamics of prolate spheroid objects in a channel consists of a series of time-periodic equilibrium states with marginal steady states in between.

1. INTRODUCTION

Many manufacturing processes involve transport of solid particles suspended in fluid in the form of slurries, colloids, polymers, or ceramics. For cases where the particle's inertia can be neglected, the dynamics of single particle motion, interaction with other particles, and effects on the bulk properties are well understood. However, in many particle transport applications, the particle inertia cannot be neglected. In these cases, the effects of particle motion and particle-particle interaction on the microstructure and the macroscopic transport behavior are not well understood. In fact, very basic information, such as the effect of inertia on interaction of two solid particles in a simple shear flow is unavailable. In order to study the fundamental effect of inertia on particle motion, particle interaction and microstructure, and effects on the bulk properties, we need to solve the full momentum equation to analyze the dynamics of individual particle suspended in the fluid. Progress has been made towards this goal by the recent finite element simulations of two-dimensional particles suspended in fluid by Feng, Hu, and Joseph (1994 a,b); Huang, Feng, and Joseph (1994), and Feng and Joseph (1995). These results provide considerable information on the particle motion and interaction at finite particle Reynolds number. Their finite element simulation is based on solution of the Navier-Stokes equation for the fluid domain using a commercial software, POLYFLOW. The procedure involves computation of the net force and torque on the solid particle, explicit translation and rotation of the particle, remeshing, and projection of the solution from the previous time step onto the remeshed computational domain at every time step (Hu et.al., 1992). Up to date, only 2-D solutions have been reported due to the excessive computational time required by this approach. Analysis of 3-D problems involving transport of solid particles require a more efficient computational method.

We take a different approach which we believe is more efficient than convential method. Our approach is to solve the discrete Boltzmann equation for the fluid phase as it is coupled, through fluid-solid interaction rules, to the translation and rotation of the solid particles suspended in the fluid. The discrete Boltzmann equation treats the continuum fluid phase as a set of fluid particles which move in discrete directions. It is well established that with an appropriate equilibrium distribution function, the discrete Boltzmann equation will reduce to the Navier-Stokes equation (McNamara and Zanetti, 1988; Chen et al., 1992; Hou et al., 1995). The advantage of this approach is based on the local nature of the computations, that is numerical communications between the computational nodes are with immediate neighbors only. Furthermore, there is no need for solution of linear systems. Therefore, this method can be

* Author to whom correspondence should be addressed.

efficiently implemented on parallel processors. That is the computational domain can be divided and distributed on many processors with little communication between each processor. We demonstrate the advantage of this approach in the last section of this paper by presenting results of computational time required for 3-D simulations.

Application of the Discrete Boltzmann method to analysis of particles suspended in fluid is a natural extension of this approach. This idea was first proposed by Ladd et al. (1988), who used the lattice-gas approach, and later, the lattice-Boltzmann method (Ladd, 1994) to simulate transport of pseudo-solid particles with an interior fluid mass. In other words, Ladd's model requires fluid to cross the boundary of the suspended solid particle and occupy the entire domain such that the computational nodes inside and outside the solid particle are treated in an identical manner. This method is accurate in most situations where inertia is not important. As Ladd (1994) recognized, in unsteady problems, where inertia becomes important, the fluid inside the 'solid' particles generate some error in the solution. We show that in these situations, the error accumulates in time into large deviations from the actual solution.

To have a robust and accurate computational method, we have developed a method based on the discrete-Boltzmann equation for analysis of real impermeable solid particles suspended in the fluid (Aidun and Lu, 1995). In this paper, we briefly outline the method and provide a series of comparisons with known solutions and experimental data to demonstrate the accuracy and robustness of this approach. We show that this method works well when applied to suspension flow with or without inertia for steady or unsteady flows. We compare our results with the results of Feng et al. (1994a) and Feng & Joseph (1995) for sedimentation of circular and elliptical cylinders in a channel (2-D simulations). We extend the computations to much longer times to get equilibrium solutions for particle Reynolds numbers ranging from 0.01 to 6.08. We show that an interesting set of equilibrium time-periodic states separated by marginal steady equilibrium states exist in the range of $0 < Re_p \leq 6.08$. Also, we present new results for 3-D analysis of prolate spheroids for $Re_p = 2.26$.

2. LATTICE BOLTZMANN EQUATION

In the lattice Boltzmann simulations, the fluid phase is modeled by a set of fluid particles which are distributed in a regular lattice, according to a distribution function, and move along the lattice links with discrete velocities. The distribution of fluid particles evolves according to the discrete Boltzmann equation. It has been established that the full Navier-Stokes equation can be recovered from this system (McNamara and Zanetti, 1988; Chen et.al., 1992).

We use a three speed lattice-Boltzmann model where the fluid particles can be at rest or can move along the horizontal/vertical and the diagonal directions. The velocity vectors are denoted as $\mathbf{e}_{01}$ for the fluid particles at rest, $\mathbf{e}_{1i}$ and $\mathbf{e}_{2i}$ for the fluid particles moving along the non-diagonal and diagonal directions, respectively. The velocity vectors are defined as

$$\mathbf{e}_{01} = (0,0), \tag{1}$$

$$\mathbf{e}_{1i} = (\cos\frac{i-1}{2}\pi, \sin\frac{i-1}{2}\pi), \quad i = 1,\cdots,4, \tag{2}$$

$$\mathbf{e}_{2i} = \sqrt{2}(\cos(\frac{i-1}{2}\pi + \frac{\pi}{4}), \sin(\frac{i-1}{2}\pi + \frac{\pi}{4})), \quad i = 1,\cdots,4, \tag{3}$$

where the value of i refers to each of the four diagonal or non-diagonal directions. The lattice Boltzmann equation is given by

$$f_{\sigma i}(\mathbf{x} + \mathbf{e}_{\sigma i}, t+1) - f_{\sigma i}(\mathbf{x}, t) = -\frac{1}{\tau}[f_{\sigma i}(\mathbf{x}, t) - f^{(0)}_{\sigma i}(\mathbf{x}, t)], \tag{4}$$

where $f_{\sigma i}(\mathbf{x}, t)$ $(\sigma = 0, i = 1; \sigma = 1, 2, i = 1, \cdots, 4)$ represents the single-particle distribution function, $f^{(0)}_{\sigma i}(\mathbf{x}, t)$ is the equilibrium distribution function, and τ is the single relaxation time. In our simulations, $f^{(0)}_{\sigma i}(\mathbf{x}, t)$ is taken as

$$f^{(0)}_{\sigma i}(\mathbf{x}, t) = \rho(\mathbf{x})[A_\sigma + B_\sigma(\mathbf{e}_{\sigma i} \cdot \mathbf{u}) + C_\sigma(\mathbf{e}_{\sigma i} \cdot \mathbf{u})^2 + D_\sigma u^2], \tag{5}$$

where $\rho(\mathbf{x})$ is the fluid particle density at the node, and the constants in (5) are given by

$$\begin{aligned} &A_0 = \frac{1}{2}, \quad B_0 = 0, \quad C_0 = 0, \quad D_0 = 0, \\ &A_1 = \frac{1}{12}, \quad B_1 = \frac{1}{3}, \quad C_1 = \frac{1}{2}, \quad D_1 = -\frac{1}{2}, \\ &A_2 = \frac{1}{24}, \quad B_2 = \frac{1}{12}, \quad C_2 = \frac{1}{8}, \quad D_2 = \frac{1}{8}. \end{aligned} \tag{6}$$

For this model, the parameter $c_s = \sqrt{1/3}$, and the kinematic viscosity is $\nu = (2\tau - 1)/6$. The density and the macroscopic velocity are obtained from the first two moments, given by

$$\begin{aligned} \rho(\mathbf{x}, t) &= \sum_{\sigma,i} f_{\sigma i}(\mathbf{x}, t), \\ \rho(\mathbf{x}, t)\mathbf{u}(\mathbf{x}, t) &= \sum_{\sigma,i} f_{\sigma i}(\mathbf{x}, t)\mathbf{e}_{\sigma i}, \end{aligned} \tag{7}$$

respectively. In 3-D, the fluid phase is modeled by a group of fluid particles moving in a simple cubic lattice with discrete velocities. There are 19 different velocities which fall

into three categories according to their magnitudes. Each category has the same magnitude but different directions. The velocity vectors are denoted as $\mathbf{e}_{\sigma i}$ with $\sigma = 0, 1, 2$. Table 1 lists all 19 different velocity vectors. With these 19 velocities, at each time step, the moving fluid particles leave the original node and arrive at the nearest node along a given direction. The distribution of fluid particles evolve according to the distribution function $f_{\sigma i}(\mathbf{x}, t)$ ($\sigma = 0, i = 1; \sigma = 1, i = 1, \cdots, 6; \sigma = 2, i = 1, \cdots, 12$). The constants for the equilibrium distribution function, $f^{(0)}_{\sigma i}(\mathbf{x}, t)$ in 3-D applications are given by

$$
\begin{aligned}
&A_0 = \frac{1}{4}, \quad B_0 = 0, \quad C_0 = 0, \quad D_0 = 0, \\
&A_1 = \frac{1}{12}, \quad B_1 = \frac{1}{6}, \quad C_1 = \frac{1}{4}, \quad D_1 = -\frac{1}{4}, \\
&A_2 = \frac{1}{48}, \quad B_2 = \frac{1}{12}, \quad C_2 = \frac{1}{8}, \quad D_2 = 0.
\end{aligned}
\tag{8}
$$

The parameter c_s and kinematic viscosity have the same values as for the 2-D case defined above.

Table 1: List of 19 velocities

k	σ	i	$\mathbf{e}_{\sigma i}$	$\lvert\mathbf{e}_{\sigma i}\rvert$
0	0	1	(0,0,0)	0
1	1	1	(1,0,0)	1
2	2	1	(1,1,0)	$\sqrt{2}$
3	1	2	(0,1,0)	1
4	2	2	(-1,1,0)	$\sqrt{2}$
5	1	3	(-1,0,0)	1
6	2	3	(-1,-1,0)	$\sqrt{2}$
7	1	4	(0,-1,0)	1
8	2	4	(1,-1,0)	$\sqrt{2}$
9	2	5	(1,0,1)	$\sqrt{2}$
10	2	6	(0,1,1)	$\sqrt{2}$
11	2	7	(-1,0,1)	$\sqrt{2}$
12	2	8	(0,-1,1)	$\sqrt{2}$
13	1	5	(0,0,1)	1
14	2	9	(-1,0,-1)	$\sqrt{2}$
15	2	10	(0,-1,-1)	$\sqrt{2}$
16	2	11	(1,0,-1)	$\sqrt{2}$
17	2	12	(0,1,-1)	$\sqrt{2}$
18	1	6	(0,0,-1)	1

3. BOUNDARY RULE AND DYNAMICS OF PARTICLES

In the lattice Boltzmann simulation of suspension flows, the solid particles move in a continuous way based on the Newtonian dynamics principles. The boundary of a solid particle is defined by a set of lattice nodes which are located on the solid boundary adjacent to the interface between the solid and the fluid. Each of these solid-boundary nodes has at least one lattice link connecting to a fluid node, that is a node in the fluid domain. The fluid nodes with at least one link connecting to a solid-boundary node are the fluid-boundary nodes. The boundary conditions at the solid surface are imposed along the links connecting the two sets of solid and fluid boundary nodes. The transfer of momentum between the fluid and the solid object also occurs along the lattice links that connect the solid-boundary node to the fluid-boundary nodes. We refer to these links as the boundary links.

The boundary condition imposed at the solid-fluid interface is the no-slip condition; that is, the fluid adjacent to the solid surface moves at the same velocity as the solid surface. The solid boundary is always assumed to be at the middle point of the boundary link. In this case, the fluid particles impact the solid boundary in the middle of the convection process and exchange momentum with the solid object (Fig.1). Ladd (1994) provides a relation for the exchange of momentum between the fluid and the solid boundary nodes. As mentioned before, he assumes that the fluid particles can occupy the entire domain including the volume of the solid particle. The fluid inside the solid particle exerts a time-dependent force on the solid particle (Ladd, 1994) based on the particle's inertia which is influenced by the fluid inertia inside the particle.

We have developed a method which does not require transfer of fluid into the solid particle and, therefore, applies to real suspensions (Aidun and Lu, 1995; Aidun et al., 1997). Here we only briefly outline our method, for more details, refer to Aidun et al. (1997). In this method the force on the solid particle consists of the body force and the hydrodynamic force exerted on the surface from the nodes outside the solid boundary which are occupied by fluid. The nodes inside the solid boundary are solid nodes and, therefore, contain no fluid. Consequently, the transfer of momentum is only between the solid boundary and the adjacent fluid. The force on the solid particle along the boundary link (σi) is given by

$$
\mathbf{F}_{\sigma i}(\mathbf{x}, t + \frac{1}{2}) = 2[f_{\sigma i}(\mathbf{x}, t) + \rho B_\sigma \mathbf{u}_b \cdot \mathbf{e}_{\sigma i'}]\mathbf{e}_{\sigma i}, \tag{9}
$$

and the particle distribution function along the bounce-back links at the solid boundary is given by

$$
f_{\sigma i'}(\mathbf{x}, t + 1) = f_{\sigma i}(\mathbf{x}, t_+) + 2\rho B_\sigma \mathbf{u}_b \cdot \mathbf{e}_{\sigma i'} + \epsilon_\sigma \delta\rho, \tag{10}
$$

where i is the direction toward the solid boundary along the boundary links and i' is the opposite direction, as shown in Fig.1. Here $\delta\rho$ is the total 'extra mass' at the boundary node and ϵ_σ is a constant (Aidun and Lu, 1995).

The purpose for the isotropic term '$\epsilon_\sigma \delta\rho$' in (10) is to locally balance the mass around the solid particle. Previously, we (Aidun and Lu, 1995) used this term to impose a node-wise mass balance using the rest particles (i.e., $\epsilon_0 \neq 0$ and $\epsilon_1 = \epsilon_2 = 0$). A simpler and more efficient approach is to only require a net mass balance around a moving solid particle. With this approach, $\epsilon_\sigma = 0$; and the density for a new fluid node uncovered due to the motion of the solid particle is obtained with the following relation

$$\rho(\mathbf{x}_b, t+1) = \frac{1}{N_b} \sum_{N_b} \rho(\mathbf{x}_b + \mathbf{e}_{\sigma j}, t_+), \qquad (11)$$

where subscript b denotes a new boundary node and N_b is the number of nodes adjacent to the uncovered boundary node. This relation states that the fluid particle density of the new node is equal to the average fluid particle density of its neighboring nodes. The macroscopic velocity of the new boundary node is equal to the solid boundary node at the time step when it is uncovered. These values are used in (5) to compute the equilibrium distribution function $f_{\sigma i}^{(0)}(\mathbf{x}_b, t+1)$, for the newly uncovered boundary node. For future time steps, the mass and macroscopic velocity of the boundary nodes are computed based on Eqs.(4) and (10). We believe that the simpler approach presented here is more accurate and robust than the methods presented by Ladd (1994) or by Aidun and Lu (1995).

The macroscopic boundary velocity vector $\mathbf{u}_b$ used in the boundary rule is obtained from the translational velocity, $\mathbf{U}$, and the angular velocity, $\mathbf{\Omega}$, of the solid particle; that is

$$\mathbf{u}_b(\mathbf{x}, t) = \mathbf{U}(t) + \mathbf{\Omega}(t) \times (\mathbf{x} + \frac{1}{2}\mathbf{e}_{\sigma i} - \mathbf{X}), \qquad (12)$$

where $\mathbf{x}$ is the position vector from center of mass to the respective node on the boundary, and $\mathbf{X}$ is the position vector of the center of mass in the inertial frame.

For a given link (σi) on a fluid-boundary node, the force on the solid particle is given by

$$\mathbf{F}_{\sigma i} = \begin{cases} 2(f_{\sigma i} + \rho B_\sigma \mathbf{u}_b \cdot \mathbf{e}_{\sigma i'})\mathbf{e}_{\sigma i}, & \text{boundary link,} \\ 0, & \text{otherwise,} \end{cases} \qquad (13)$$

whereas the torque, $\mathbf{T}_{\sigma i}$, with respect to the center of mass, $\mathbf{X}$, is given by

$$\mathbf{T}_{\sigma i} = (\mathbf{x} + \frac{1}{2}\mathbf{e}_{\sigma i} - \mathbf{X}) \times \mathbf{F}_{\sigma i}. \qquad (14)$$

With the net force and the torque calculated from the above equations, the motion of the solid particle is determined by solving Newton's equations as follows:

$$M\frac{d\mathbf{U}}{dt} = \sum_{FBN} \sum_{\sigma} \sum_{i} \mathbf{F}_{\sigma i}(\mathbf{x}, t), \qquad (15)$$

for translation where FBN stands for the fluid-boundary nodes, and,

$$\mathbf{I} \cdot \frac{d\mathbf{\Omega}}{dt} + \mathbf{\Omega} \times (\mathbf{I} \cdot \mathbf{\Omega}) = \sum_{FBN} \sum_{\sigma} \sum_{i} \mathbf{T}_{\sigma i}(\mathbf{x}, t), \qquad (16)$$

for rotation of the solid particles. Here M is the mass of the suspended particle, and $\mathbf{I}$ and $\mathbf{\Omega}$ are the inertia tensor and angular velocity. The above two equations completely prescribe the motion of the suspended solid particles in the fluid. These equations are solved using a 4th order accurate Runge-Kutta integration procedure. In the following sections, we use several examples to show the accuracy and reliability of this method. For more detailed outline of the computational method, refer to Aidun et.al. (1997).

4. RESULTS

Several 2-D and 3-D cases are analyzed in this section to examine the accuracy of this method. The 2-D results are for analysis of cross-flow over a circular cylinder in a channel, the rotation of an ellipse in a simple shear flow, the sedimentation of a circular cylinder in a channel, and the sedimentation of two ellipses in a channel. The 3-D results are for sedimentation of a sphere inside a square channel and sedimentation of two prolate spheroids in a large rectangular channel.

The governing equations for particle motion in fluid are the usual Navier-Stokes and continuity equations complemented by the Newtonian Dynamics equation for the motion of the solid particle. In non-dimensional form, these equations are given by

$$Re\left(\frac{\partial \mathbf{u}}{\partial t} + \mathbf{u} \cdot \nabla \mathbf{u}\right) = -\nabla p + \nabla^2 \mathbf{u}, \qquad (17)$$

$$\nabla \cdot \mathbf{u} = 0, \qquad (18)$$

$$\alpha q Re \frac{d\mathbf{V}}{dt} = \mathbf{f} + q(\alpha - 1) Fr^{-1} Re, \qquad (19)$$

where length, velocity, time, and force are scaled by d, U, d/U, and $\mu U d$, respectively. There are four parameters in this equation that influence the flow. These are the Reynolds number, $Re = \rho U d/\mu$, the solid to fluid density ratio, $\alpha = \rho_s/\rho$, the Froud number, $Fr = U^2/gd$, and the shape parameter, $q = m/\rho_s d^n$, where m is the mass of the solid particle. For 2-D cases, m and force are per unit length, and therefore, $n = 2$; for 3-D cases, $n = 3$. The magnitude of the hydrodynamic surface force, $\mathbf{f}$, and the body force due to buoyancy, the second term on the RHS of (19), determine the acceleration and the equilibrium state of the suspended particle. In particle sedimentation problems, as $Re \to 0$, the parameter Re/Fr has to remain finite.

The quasi-steady approximation for particle motion neglects the fluid, as well as, the solid inertia. The governing equations (17)-(19) reduce to

$$\nabla p = \nabla^2 \mathbf{u}, \quad \nabla \cdot \mathbf{u} = 0, \quad \mathbf{F} = 0, \tag{20}$$

where $\mathbf{F}$ is the sum of forces on the solid particle. Feng and Joseph (1995) use $(m/\mu U)^{1/2}$ to scale time instead of d/U and rewrite (17)-(19) as

$$\left(\frac{\rho d^3}{m}\right)^{1/2} Re^{1/2} \frac{\partial \mathbf{u}}{\partial t} + Re\mathbf{u} \cdot \nabla \mathbf{u} = -\nabla p + \nabla^2 \mathbf{u}, \tag{21}$$

$$\nabla \cdot \mathbf{u} = 0, \tag{22}$$

$$\left(\frac{m}{\rho d^3}\right)^{1/2} Re^{1/2} \frac{d\mathbf{V}}{dt} = \mathbf{F}. \tag{23}$$

This results in $Re^{-1/2}$ larger scale for the $\partial \mathbf{u}/\partial t$ term than the convective term $\mathbf{u} \cdot \nabla \mathbf{u}$. They then state that for small but finite Re, it may be more appropriate to only neglect order Re terms and retain the fluid and particle inertia terms that are order $Re^{1/2}$.

In our computations, we include all of the inertia and viscous terms regardless of the value of Re. We examine the behavior of particle motion and sedimentation for $0 < Re \leq 6.08$.

4.1 Flow Over a Circular Cylinder in a Channel (2-D), $Re_p = 1$

A circular cylinder moves along the centerline of a channel with velocity U, as shown in Figures 2. To solve for the velocity and pressure profile, one can either fix the coordinate system with the cylinder (Fig. 2a) or the wall (Fig. 2b). The Navier-Stokes equations, being Galilean invariant, give exactly the same velocity and pressure profile for these two cases.

The computational domain is 64×64 lattice units. Periodic boundary conditions are applied at the sides of the domain and no-slip conditions are imposed along the solid surfaces. The channel width is $6d$, where d is the diameter of the cylinder. The particle Reynolds number, Re_p, defined as Ud/ν is 1 (ν is the kinematic viscosity).

We solve these two cases with the discrete Boltzmann equation using the method outlined in the previous section for the moving solid particle of case b. The results for the velocity profile and the pressure distribution along the surface of the cylinder for each case are presented in Figures 3 and 4, respectively. There is perfect agreement for the solution of the two cases showing that the solid-fluid boundary rule for moving objects, outlined above, gives the same result as the solution of the Boltzmann equation for stationary boundaries. We have also compared the results from Ladd's method with our simulations and show that for this case, since the flow is steady state, the results are the same.

4.2 Rotation of an Ellipse in a Simple Shear Flow at $Re \ll 1$:Comparison with Jeffery's solution

Motion of an ellipsoid $(x^2/a^2 + y^2/b^2 + z^2/c^2 = 1)$ in a simple shear flow is analyzed by Jeffery (1922) for the vanishing particle Reynolds number. To examine the results from our computational analysis, we solve for the motion of a 2-D elliptical cylinder. This case corresponds to one of Jeffery's special solutions, given by

$$\chi = \tan^{-1}\left(\frac{b}{c}\tan\frac{bc\dot{\gamma}t}{b^2+c^2}\right),$$

$$\dot{\chi} = \frac{\dot{\gamma}}{b^2+c^2}(b^2\cos^2\chi + c^2\sin^2\chi),$$

where χ and $\dot{\chi}$ are the angle and the angular rate of the rotation, $\dot{\gamma}$ is the shear rate and t represents time. In this problem, one of the ellipsoid's principle axis, x, is always parallel to the shear field vorticity vector. This solution also applies to a 2-D ellipse which is the limit of an ellipsoid with one principle axis extended to infinity.

Our computational domain is 640×320 lattice nodes. We consider the full momentum equation at $Re_p = \dot{\gamma}b^2/\nu = 0.08$, where the major axis $b = 2c$. The computational results are compared to Jeffery's solution in Fig. 5 with very good agreement. Further decrease in particle Reynolds number in our computation results in a perfect overlap of the two solutions.

4.3 Sedimentation of a Circular Cylinder in a Channel (2-D)

In this section, we consider the sedimentation of a single circular particle in a narrow channel. Recently, Feng et. al. (1994a) have simulated this problem by directly solving the Navier-Stokes equations for fluid, and Newtonian dynamics equations for the solid particles. They found that if the density ratio is close to 1, and the terminal velocity of the particle is small, the particle enters a damped oscillation and then reaches its steady state.

In our computational analysis, we used the same conditions as Feng, et. al. (1994a). That is, a circular particle of diameter d is released in a vertical channel of width $L = 1.5d$ which then settles under gravity. The initial position of the particle is off the centerline of the channel. The density ratio of solid to fluid is 1.3. The inlet of the domain where zero velocity is applied uniformly is always $10d$ from the upstream side of the moving particle, whereas the downstream boundary is $15d$ from the particle. The normal derivative of velocity is set to zero at the downstream boundary. Fig.6 shows the lateral motion of the particle

for both the present model and Ladd's model. As comparison, some typical data points from Feng, et. al.(1994a) are also shown in Fig.6. The present model gives a damped oscillation which is in agreement with Feng's simulation, while Ladd's model shows a significant phase difference after the first cycle. Since the transient process is important in this system, the fluid inside the particle in Ladd's model results in a significant error.

In conclusion, the new boundary rule presented above and in Aidum et.al.(1997) is accurate for unsteady as well as steady state problems. We have a number of additional comparisons for this case which are presented in Aidun & Lu(1995).

4.4 Sedimentation of a sphere in a channel (3-D)

In this section, we present results for the sedimentation of a single spherical particle in a long square channel. A spherical particle of diameter d is released in a vertical square channel of width L which then settles under gravity. The sphere is initially released at the center of the cross section of the channel with zero velocity. The particle settles along the axis of the channel and reaches its terminal velocity. With the walls at a finite distance from the particle, the terminal velocity will be less than the terminal velocity of an unconfined particle. Aidun and Lu (1995) have analyzed the 2-D version of this problem for $0 < Re < 3.3$ and compared their results with the numerical results of Feng et.al., (1994) with perfect agreement in all cases. Here, we present results from analysis of the 3-D problem and we compare our results with the experiments of Miyamura et. al. (1981) who give a correlation for a best fit to their experimental data points. We have not been able to find any other 3-D computational simulations of this problem. With the new model, the lattice Boltzmann simulation has been carried out for the 3-D sedimentation in the same conditions as the experiments. In our analysis, the channel is divided into $1024 \times 64 \times 64$ lattice units. The inlet of the domain where zero velocity is applied uniformly is always 400 lattice units away from the particle, whereas the downstream boundary is 624 lattice units downstream from the particle. The normal derivative of velocity is set to zero at the downstream boundary. We also include results of a coarser grid, $512 \times 32 \times 32$, for evaluating the effect of computational resolution. The wall effect is defined as

$$\xi = u_t/u_0$$

where u_t is the terminal velocity with nearby boundary walls, and u_0 is the unconfined terminal velocity from Stokes equation. Fig. 7 shows a comparison of the results from our computational analysis with the best curve fit to the experimental data of Miyamura et. al. (1981). As shown in this figure, there is good agreement between the experiments and our computational results.

4.5 Sedimentation of two ellipses in a channel (2-D)

The dynamics of two identical ellipses sedimenting in a long channel shows interesting behavior. Feng and Joseph (1995) studied this problem at $Re \ll 1$ by direct solution of the steady as well as the unsteady Stokes equation. They show that the results computed from the unsteady Stokes equation is qualitatively different from the steady Stokes equations using quasi-steady approximations as in Stokesian Dynamics (Brady and Bosis, 1988; Claeys and Brady, 1993).

The ellipse have an aspect ratio of 2:1 where major axis is d. They are released at $t = 0$ from a vertical orientation (i.e., initially the major axis is parallel to the direction of gravity) with initial center-to-center distance $2s = d$. The halfway separation point is at the center of the channel which is a symmetry plane. Similar to Feng and Joseph (1995), we use a computational domain that $10d$ wide and $25d$ high. The computational domain moves with the particle in such a way to always keep the particles' center $10d$ above the bottom boundary. As mentioned before, we include all of the viscous, inertia and body force in our computations. To compare with the results of Feng and Joseph (1995), we include a small Re case in the computations.

The results for center-to-center separation and angular rotation for $Re = 0.01$, 0.12, 0.47, 1.09, and 6.08 are presented in Figures 8a-f, respectively. The particle configuration for these cases is presented in Fig.9. Here the density ratio, $\alpha = 1.003$, shape factor $q = \pi/8$, and the Froude number, Fr, depends on the terminal velocity. For small Re the results are compared to finite element computations of Feng and Joseph (1995) in Fig.8a with perfect agreement. The ellipse rotate in a periodic state as they settle inside the channel. For our case with $Re = 0.01$, we see that the weak inertia present in the system results in a slight increase in net separation after each cycle. Eventually the particles drift away from the time-periodic state represented by the limit cycle at $Re = 0$ and approach another time-periodic equilibrium state. The second limit cycle is qualitatively different since a periodic tumbling motion replaces the full somersault orbit of the particles. This behavior can be more clearly observed when$Re = 0.12$ in Fig.8b. The particles go through two complete revolutions while they drift away. The solution approaches a stable limit cycle at $x/d = 75$. At $Re = 0.4 - 0.7$, the particle make only one full revolution before approaching an equilibrium state.

The results suggest the following mechanism. At $Re = 0$, the system instantaneously approaches an equi-

librium state, which in this case, is a full revolution time-periodic state, a 'somersault' limit cycle. There is a turning point in the solution at $Re = 0$, that is the somersault limit cycle solution ceases to exist at $Re > 0$. This is due to the particle inertia which has a commulitative effect, eventually large enough to prevent full particle rotation.

At Reynolds number about 1 and higher the particle motion quickly reaches another qualitatively different equilibrium state, as shown in Figures 8e,f and 8e,f. The large periodic meadoring motion of the particle seen at small Re is suppressed at $Re \geq 1$. In this range of Reynolds number, we see transitional regions of steady state which exists in between various periodic modes. The physics of this problem will be discussed more thoroughly in future (Aidun et.al., 1997).

4.6 Sedimentation of two prolate spheroids in a channel (3-D)

The computational domain for analysis of a pair of prolate spheroids sedimentating in a channel is equal to $25d \times 10d \times 5d$. These are more than 5×10^6 lattice nodes ($400 \times 160 \times 80$) to accurately resolve the domain. The particle Reynolds number is $Re = 2.26$ and the other parameters and boundary conditions are the same as in the 2-D cases of section 4.3. As the solid particles start their descend, they gradually go through a $\pi/2$ rotation and take on a horizontal configuration with slight amount of wobbling as shown in Fig.10. It is interesting to note that similar to the 2-D case, at larger Reynolds number, the ellipses fall in a horizontal configuration. The computational time for computational analysis particle sedimentation from $x/d = 0$ to 75 using 64 processors is about 6 hours. We expect to improve the performance on SP2 once we replace the PVM routine with the message passing (MPI) routine. We believe that the computational time required for these type of numerical analysis would be considerably larger.

ACKNOWLEDGMENTS

We acknowledge helpful discussions with Dr. J. Feng. This study has been supported by the National Science Foundation through grant CTS-9258667 and by industrial matching contributions. The 3-D computations were conducted using the parallel supercomputer system, SP2, at the Cornell Theory Center which is funded by the National Science Foundation and New York State.

REFERENCES

Aidun, C.K. and Lu, Y., 1995, "Lattice Boltzmann simulation of solid particles suspended in fluid," *J. Stat. Phys.*, **81**, p49.

Aidun, C.K. Lu,Y., and Ding,E., under preparation1997.

Brady, J.F. and Bossis, G., 1988, "Stokesian Dynamics," *Annual Rev. Fluid Mech.*, **20**, p111.

Chen,H., Chen,S., and Matthaeus,W.H., 1992, "Recovery of the Navier-Stokes equations using a lattice-gas Boltzmann method," *Physical Review A*, **45**, R5339.

Claeys,I.L. and Brady,J.F., 1993, "Suspensions of prolate spheroids in Stokes flow, Part 1, Dynamics of a finite number of particles in an unbounded fluid," *J. Fluid Mech.*, **251**, p411.

Feng, J., Hu, H.H., and Joseph,D.D., 1994a, "Direct simulation of initial value problems for the motion of solid bodies in a Newtonian fluid, Part 1, Sedimentation," *J. Fluid Mech.*, **261**, p95.

Feng, J., Hu, H.H., and Joseph,D.D., 1994b, "Direct simulation of initial value problems for the motion of solid bodies in a Newtonian fluid, Part 2, Couette and Poiseuille flows," *J. Fluid Mech.*, **277**, p271.

Feng, J., and Joseph, D.D., 1995, "The unsteady motion of solid bodies in creeping flows," *J. Fluid Mech.*, **303**, p83.

Hou,S., Zou, Q., Chen, S., Doolen, G., and Cogley, A.C., 1995, "Simulation of cavity flow by lattice Boltzmann method," *J. Computational Physics*, **118**, p329.

Hu, H.H., Crochet, M.J., and Joseph,D.D., 1992, "Direct simulation of fluid particle motions," *Theor. Comput. Fluid Dyn.*, **3** p.285.

Hu, H.H., 1996, "Direct simulation of flows of solid-liquid mixtures," *Int. J. Multiphase Flow*, **22**, p335.

Huang,Y., Feng,J., and Joseph,D.D., 1994, "The turning couple on an elliptic particle settling in a vertical channel," *J.Fluid Mech.*, **271** p1.

Jeffery, G. B., 1922, "The motion of ellipsoidal particles immersed in a viscous fluid," *Proc. R. Soc. Lond.* **A 102**, p161.

Joseph, D.D., 1994, "Interrogation of numerical simulation for modeling of flow induced microstructure," in *Liquid-Solid Flows* 1994, American Society of Mechanical Engineers, **189**, p31.

Ladd,A.J.C., Colvin,M.E., and Frenkel,D., 1988, "Application of lattice-gas cellular automata to the Brownian motion of solids in suspension," *Phys. Rev. Lett.*, **60**, p975.

Ladd, A.J.C., 1994, "Numerical simulations of particulate suspensions via a discretized Boltzmann equation," Parts 1&2, *J. Fluid Mech.*, **271**, p285.

McNamara, G.R., and Zanetti, G., 1988, "Use of the Boltzmann equation to simulate lattice-gas automata," *Phys. Rev. Lett.* **61**, p2332.

Miyamura, A., Iwasaki, S., and Ishii, T, 1981, "Experiment wall correction factors of single solid spheres in triangular and square cylinders, and parallel plates," *Int. I. Multiphase Flow*, **7**, p41.

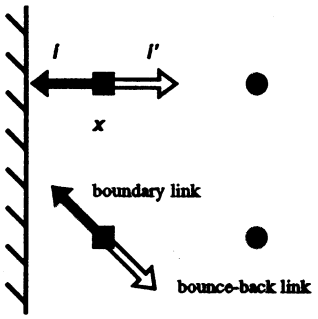

Figure 1. Location of fluid-boundary nodes denoted by solid squares adjacent to a solid surface. The boundary links are represented by solid arrows; The bounce-back links, by hollow arrows.

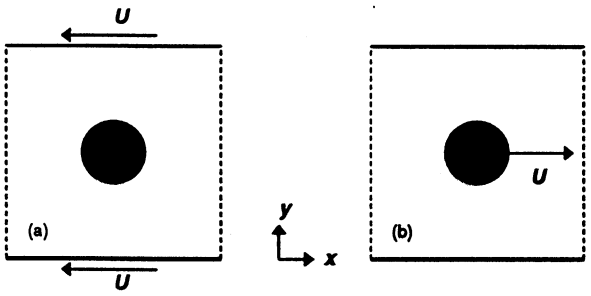

Figure 2. A circular particle moves along the center-line of a straight channel. (a) The coordinate system is fixed with the cylinder while the top and bottom walls move with a constant velocity. (b) The particle moves at the constant velocity while the walls are stationary.

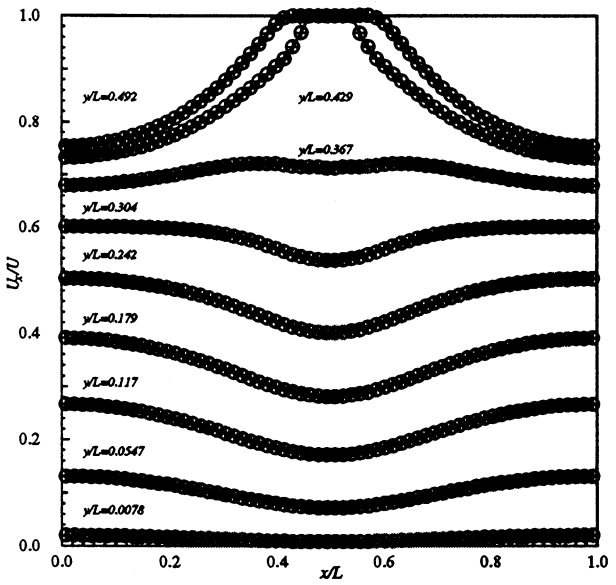

Figure 3. X component of velocity field along horizontal lines. + is for the present model applied to the moving cylinder, O is for Ladd's model. The Galilean transformed results for the case of the fixed particle are presented by the sliod lines.

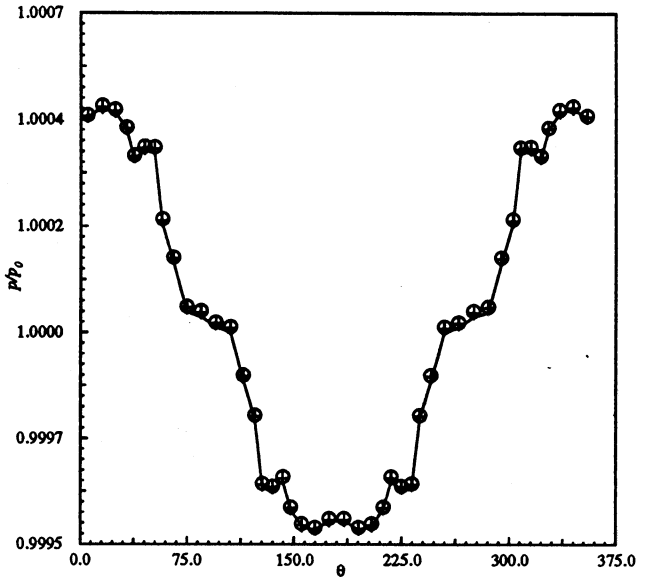

Figure 4. Angular distribution of the pressure at the interface relative to the undisturbed pressure. The angle in degree is messured from the front of the particle. + is for the present model, O is for Ladd's model. The results for the case of the fixed particle are presented by the sliod lines.

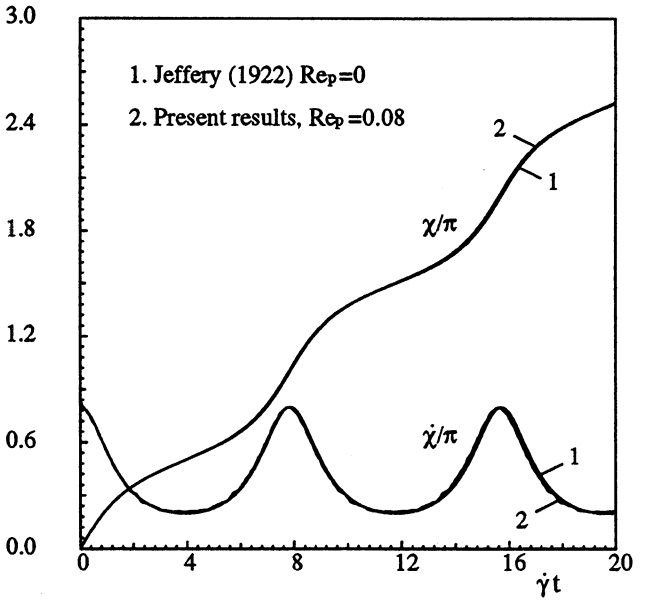

Figure 5. Rotation of an ellipse (i.e., a 2-D ellipsoid $x^2/a^2+y^2/b^2+z^2/c^2=1$, $1/a \to 0$) in a simple shear flow u=0, v=0, w=$\dot{\gamma}$y at small particle Reynolds number. Jeffery's solution is for $Re_p=0$ and our computational results are at $Re_p=0.08$.

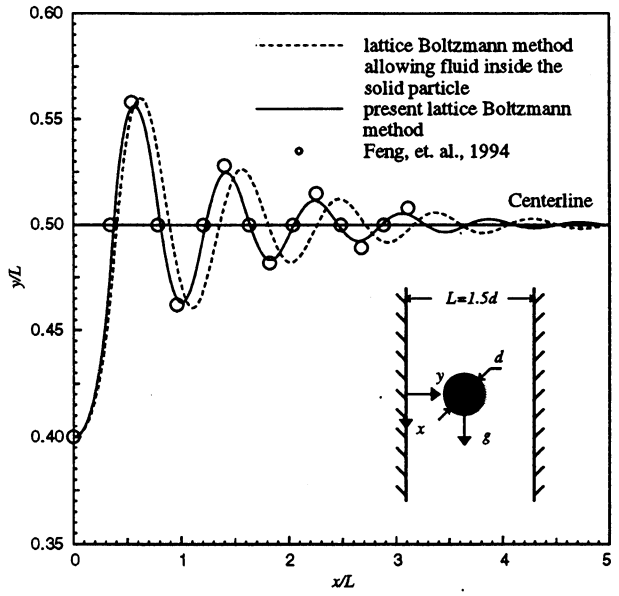

Figure 6. Settling trajectory of a circular particle with Reynolds number 6.28. Comparison between two different lattice Boltzmann models (solid and dashed lines) and the simulation results of Feng et.al., 1994 (open circles). The solid line is obtained using present lattice Boltzmann method. The dashed line is based on Ladd's (1994) method allowing fluid inside the solid particle.

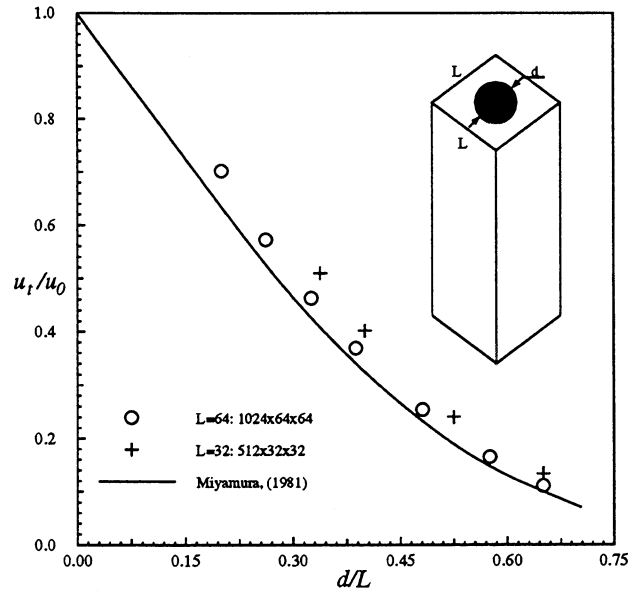

Figure 7. Wall effect on a single sphere settling in a long square channel. The solid line is a best fit to the experimental data of Miyamura. The open circles and + symbols are from our lattice Boltzmann computational analysis. The results are within the experimental error.

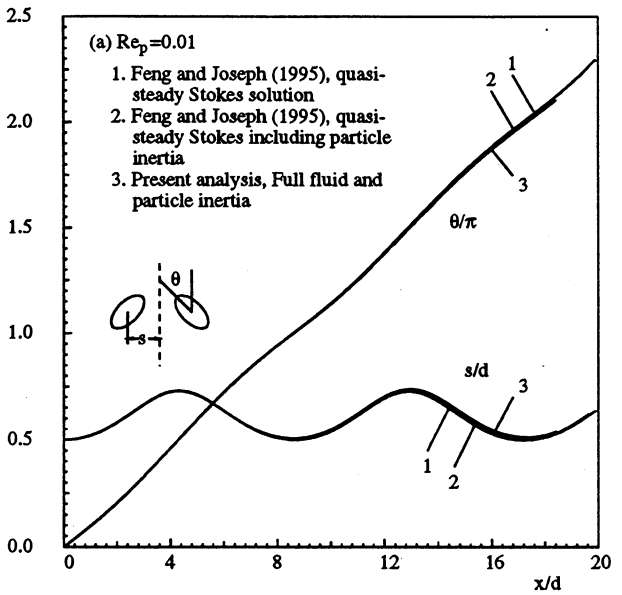

Figure 8a. Sedimentation of two identical ellipses from initial vertical orientation in an infinitely long vertical channel for Reynolds number ranging between 0.01 and 6.08. d is the length of the major axis; s is half of the center-to-center separation between two ellipses; θ is the angle of rotation from initial configuration, and x is the vertical sedimentation distance from initial position at x=0. Each plot from (a) to (f) corresponds to diagrams (a) to (f) in Fig.9, respectively. The results obtained by a quasi-steady approximation, neglecting both the fluid inertia and the particle inertia, and the results obtained in absence of fluid inertia, considering the inertia of solid particles (Feng and Joseph, 1995), are also shown in (a).

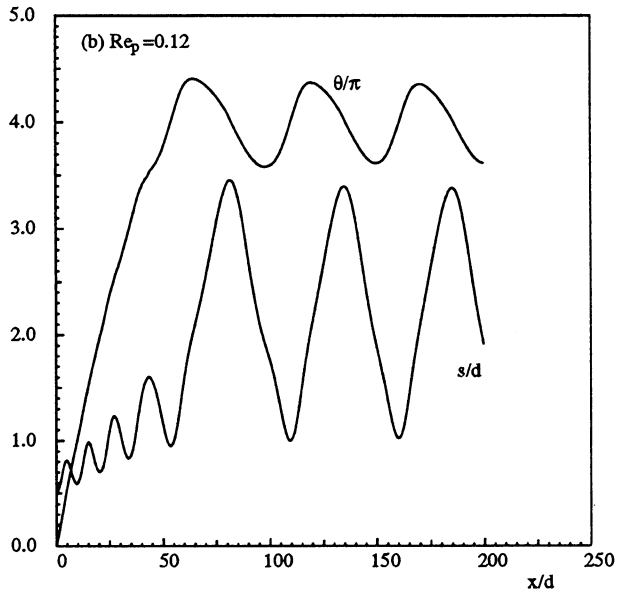

Figure 8b. See Figure 8a for caption.

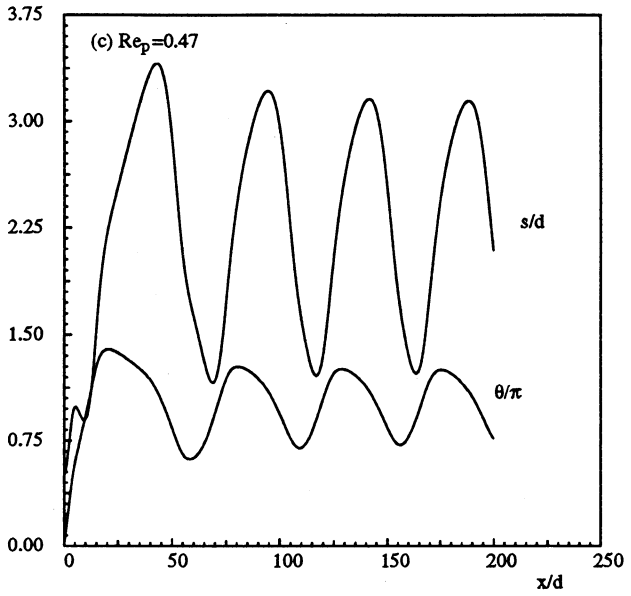

Figure 8c. See Figure 8a for caption.

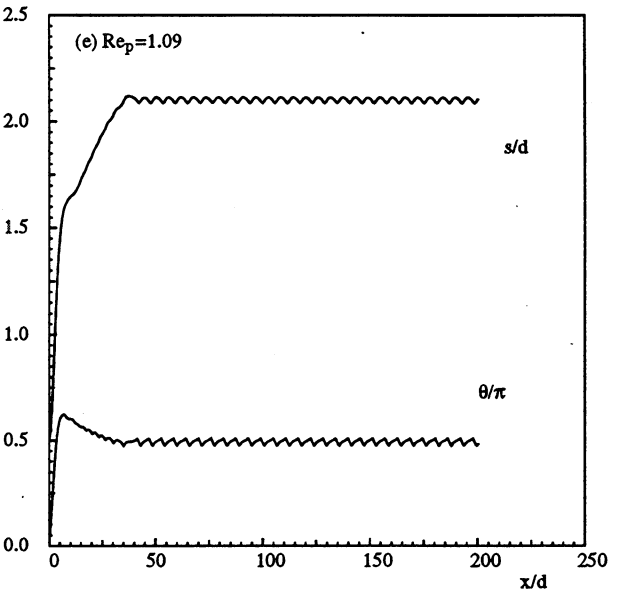

Figure 8e. See Figure 8a for caption.

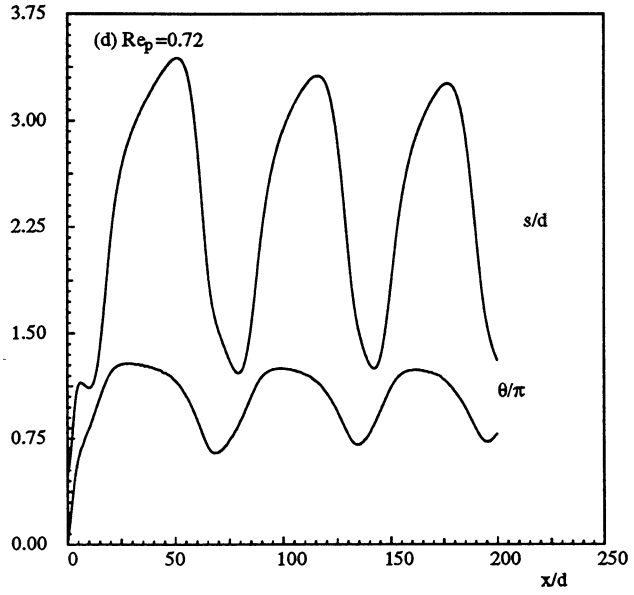

Figure 8d. See Figure 8a for caption.

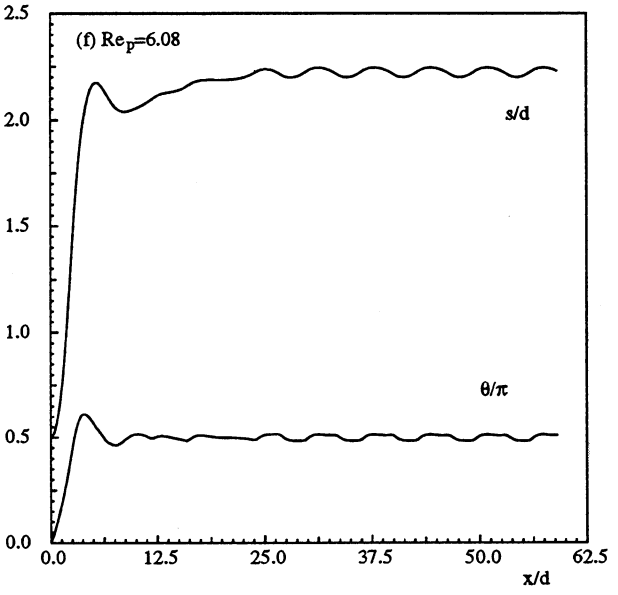

Figure 8f. See Figure 8a for caption.

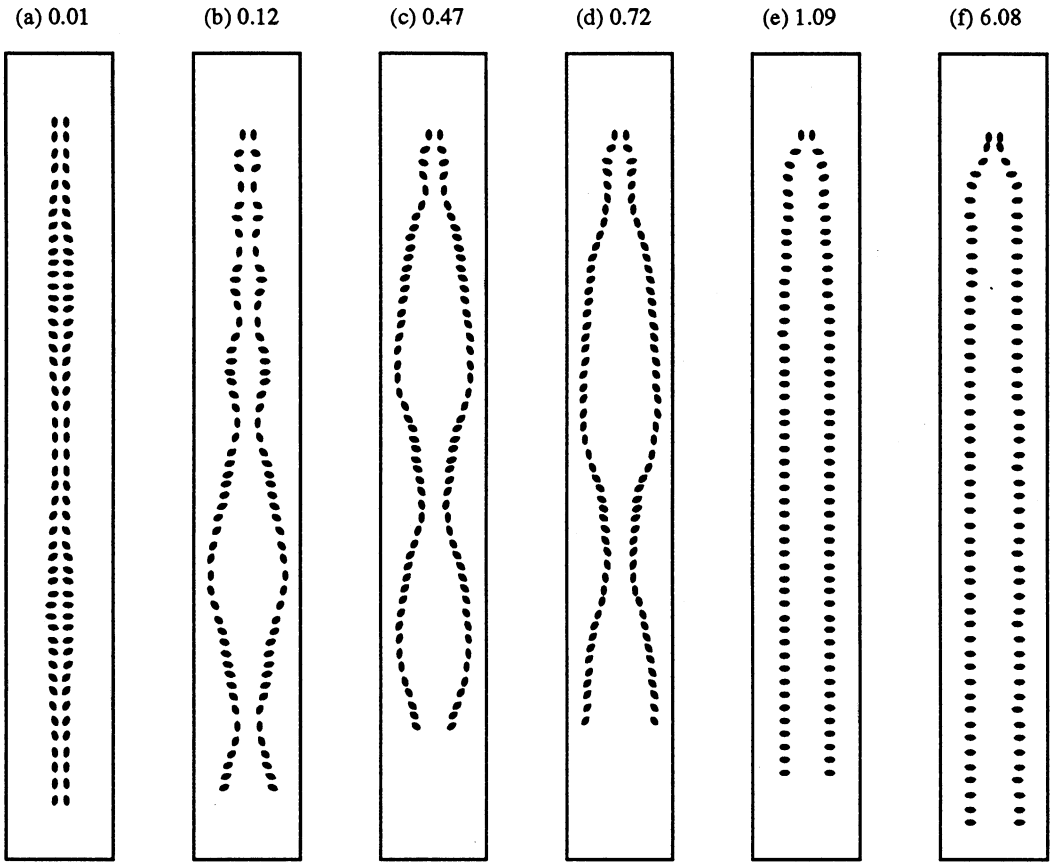

Figure 9. Snapshots of the ellipses in time during sedimentation. The Reynolds number, from 0.01 to 6.08, specified on the top of each channel, corresponds to the Reynolds number of the line plots in Fig.8.

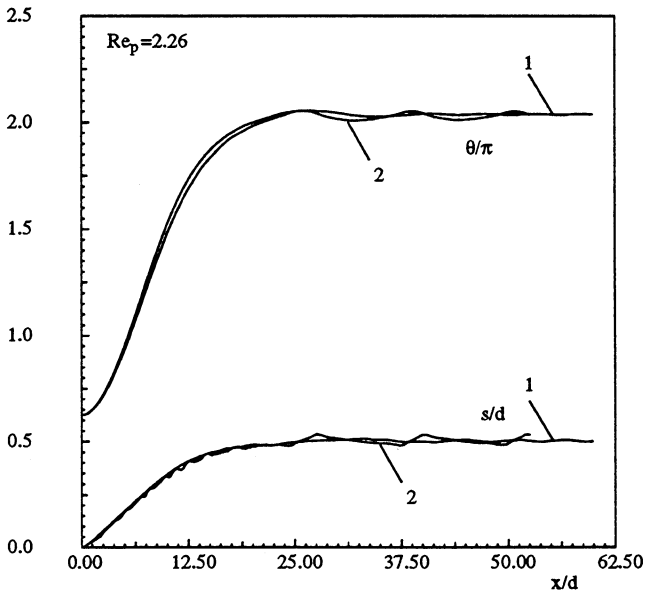

Figure 10. Sedimentation of two identical prolate spheroids from initial vertical orientation in an infinitely long vertical channel for Reynolds number 2.26. The computational domain is 25dx10dx5d discretized by 400x160x80 (1) or 200x80x40 (2) nodes.